Arch. Mech., 51, 1, pp. 71–86, Warszawa 1999

Influence of finite deformations on the growth mechanism of microvoids contained in structural metals

W. DORNOWSKI

Military University of Technology
Kaliskiego 2, 01–489 Warszawa, Poland

IN THIS PAPER an analysis of the growth mechanism of the single microvoid for finite deformations is presented. A hollow sphere model is assumed. Such a model has been considered in many previous papers, however on the assumption that the strains remain small. The material surrounding the microvoid is assumed to be work-hardening, viscoplastic, described by the constitutive equations formulated by PERZYNA [1]. Quantitative and qualitative distinctions between the presented solution and geometrically linear solution are discussed. On the basis of the obtained solution, constitutive functions of a certain damage evolution equation for the complex stress state have been identified. A numerical example of the fracture analysis for a structural element is presented.

1. Introduction

PHENOMENA such as nucleation, growth and coalescence of microvoids play a very important role in the ductile fracture process of structural metals. Domains of localized strains determine the places of void nucleation. In these domains, the voids generally nucleate by decohesion of second phase particles or by transgranular and intergranular cracking. The localized plastic deformation controls the growth and coalescence processes (neck, shear band).

Micromechanics analysis of void nucleation and coalescence, as well as of void growth, establishes the basis of constitutive modeling for porous plastic solids. Such relations play an important role in the theoretical description and in numerical analysis of the deformation and fracture processes for structural elements. Prediction of ductile fracture behavior requires the knowledge of the relation between the growth of a void and the imposed stress and strain histories.

MCCLINTOCK'S [2] analysis of the expansion of a long cylindrical hole in an ideally plastic solid marks the beginning of the recently appearing, extensive literature on the micromechanics of ductile fracture. Moreover, this paper showed that a precise mechanics analysis of a carefully chosen continuum model could help us to quantify the complex microstructural behavior. The imposed axial strain rate and the transverse stress were considered. The linearized geometri-

cal relations were assumed. McClintock's exact solution exhibits an exponential increase in the void growth rate with positive transverse stress.

RICE and TRACEY [3] analyzed the growth of an isolated spherical void surrounded by an ideally plastic matrix. This void was subjected to a general stress state. The approximate solution has been obtained by using the Rayleigh-Ritz method. The influence of viscoplastic properties of the matrix on the growth of a spherical void has been analyzed in [4]. For the limiting case (rigid-ideally plastic solid) the solution presented in [4] reduces to the solution obtained in [3]. Finite element results for the growth of an isolated spherical void in an ideally plastic solid have been obtained in paper [5]. The model of a single void immersed in the infinite material space is a characteristic mark of the void growth analysis reported in papers [2 – 5]. This approach does not take into account the void interaction effects.

A different approach taking into account void interaction effects has been presented by CAROLL and HOLT [6]. In their paper, the description of the growth mechanism has been obtained by an analysis of the collapse of a hollow sphere made of incompressible elastic-plastic material. JOHNSON [7] has analyzed the same hollow sphere model problem. The viscoplastic effects have been taken into account. Other generalizations allowed for the work-hardening effects. The void growth process for a linear, work-hardening viscoplastic material has been analyzed by PERZYNA [8]. In Perzyna's model, EFTIS and NEMES [9] have assumed the non-linear work-hardening rule. The influence of thermal effects on the growth mechanism for the discussed model has been investigated in [10].

In all papers quoted above the void growth analysis was based on the simplifying assumption that the strains in the material surrounding an isolated void remain small. In this paper we give up this assumption and consider the finite deformation of the matrix material. Such conditions can be realized in many technological problems of structural metals.

Section 2 is focused on an analysis of the growth mechanism of a single void for finite strains. The model of the hollow sphere proposed in [6] and [7] is assumed. It has been assumed that the matrix material is described by Perzyna's viscoplastic law and by the non-linear work-hardening rule. Quantitative and qualitative distinctions between the presented solution and the geometrically linearized solution [9] are discussed. In Section 3 the damage evolution equation for the complex state of stress [11] is discussed. A numerical example of fracture analysis for the structural element is presented in Section 4. The last section brings final conclusions and comments.

2. The growth mechanism of the isolated spherical void for finite deformations

We consider a rectangular volume element containing a representative distribution of voids as shown in Fig. 1. Let us assume a uniform hydrostatic tension $\overline{p}$ acting over the surface of this element [7].

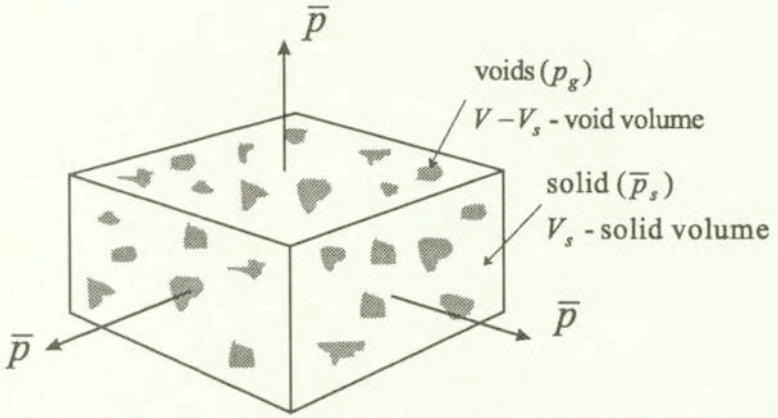

FIG. 1. Material element containing voids: $\overline{p}$ is the average mean stress acting over the element face, p_g is the gas pressure in the voids, $\overline{p}_s$ is the average mean stress in the solid material.

The equilibrium of forces acting on the cross-sectional area A occupied by the voids is expressed by the following equation [7]:

$$A_s\overline{p}_s + (A - A_s)p_g = A\overline{p}, \tag{2.1}$$

where $\overline{p}_s$ is the mean stress (spatial average) in the solid material which acts on the average area A_s on the plane of total area A, and p_g is the internal gas pressure (for reactive media). For a random distribution of hole shapes and sizes $A_s/A = V_s/V$, and we obtain that the mean stress in the solid constituent is

$$\overline{p}_s = \frac{1}{1-\xi}\overline{p} - \frac{\xi}{1-\xi}p_g, \tag{2.2}$$

where

$$\xi = \frac{V - V_s}{V} \tag{2.3}$$

is the porosity parameter describing the ratio of the voids volume to the volume of the aggregate.

A simplified model of the porous element is now assumed. Let us consider a single spherical void of initial radius a_0 in a sphere of initial radius b_0. In the

actual configuration, the void is subjected to internal pressure p_g and external stress $\overline{p}_s$ (Fig. 2.)

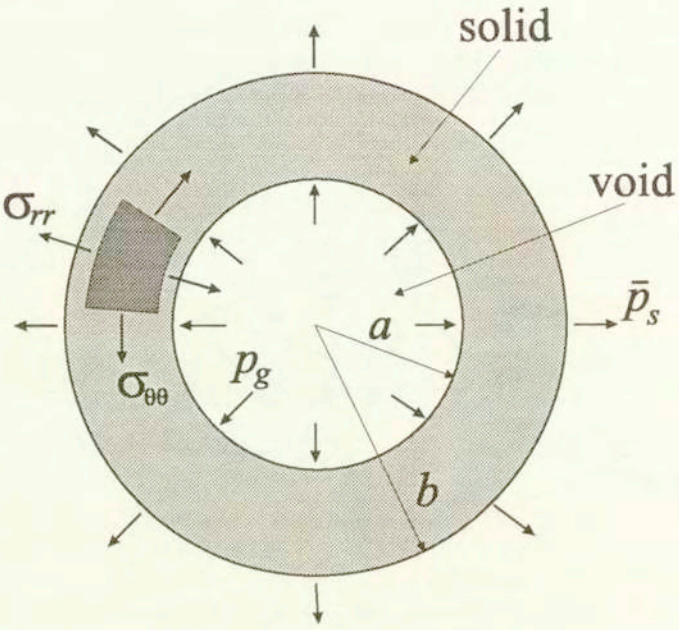

FIG. 2. Porous material model.

For these assumptions the porosity parameters, namely the initial and actual ones, are determined by relations

$$\xi_0 = \frac{a_0^3}{b_0^3}, \qquad \xi = \frac{a^3}{b^3}. \tag{2.4}$$

We carry out the analysis of the spherical void growth in the Eulerian polar coordinate system $\{r, \theta, \varphi\}$. The Lagrangian coordinates of the material point are denoted by $\{R, \Theta, \Phi\}$, and the corresponding Eulerian coordinates are as follows:

$$r = \left[R^3 + C(t)\right]^{1/3}, \qquad \theta = \Theta, \qquad \varphi = \Phi. \tag{2.5}$$

The first of the above functions of motion results from the assumption that the volume of the surrounding material has to be preserved. The integration function $C(t)$ depends only on time. The remaining functions of motion determine the conditions of spherical symmetry. Differentiating the functions (2.5) with respect to time we obtain the velocity field

$$\dot{r} = \frac{1}{3r^2}\dot{C}(t), \qquad \dot{\theta} = \dot{\varphi} = 0. \tag{2.6}$$

The spatial velocity gradient is represented by the matrix

$$\text{grad}\,\mathbf{v} = \begin{bmatrix} -\frac{2}{3r^3} & 0 & 0 \\ 0 & \frac{1}{3r^3} & 0 \\ 0 & 0 & \frac{1}{3r^3} \end{bmatrix} \dot{C}(t). \tag{2.7}$$

This matrix is symmetrical. Thus, the rotational speed of the material particle vanishes. The deformation rate tensor is equal to the spatial velocity gradient, $\mathbf{d} = \text{grad}\,\mathbf{v}$. Moreover, the incompressibility condition is satisfied, $\text{tr}\,\mathbf{d} = \text{tr}(\text{grad}\,\mathbf{v}) = 0$. The equivalent rate of deformation and equivalent deformation are as follows:

$$\dot{\bar{\varepsilon}} = \left[\frac{2}{3}(\mathbf{d}:\mathbf{d})\right]^{1/2} = \frac{2}{3r^3}\dot{C}(t), \qquad \bar{\varepsilon} = \int_0^t \dot{\bar{\varepsilon}}\,dt = \frac{2}{3}\ln\frac{r^3}{r^3 - C(t)}. \tag{2.8}$$

The equation of motion described by physical components of the Cauchy stress tensor has the form

$$\rho\ddot{r} = \frac{\partial\sigma}{\partial r} + \frac{2}{r}(\sigma_{rr} - \sigma_{\theta\theta}), \tag{2.9}$$

where ρ is the solid density. Our analysis will be restricted to the case where inertial effects are neglected, i.e. $\rho\ddot{r} = 0$. Equation (2.9) is then integrated from a to b with boundary conditions $\sigma_{rr}(a,t) = p_g$ and $\sigma_{rr}(b,t) = \overline{p}_s$, to give

$$\overline{p}_s - p_g = -2\int_a^b \frac{\Delta S}{r}dr, \qquad \Delta S = \sigma_{rr} - \sigma_{\theta\theta}. \tag{2.10}$$

The rate-dependent matrix material characterized by linear overstress function and nonlinear hardening is assumed. In this case the yield condition is given by the following relation [8]:

$$\sqrt{3J_2'} = \sigma^*\left[1 + \Phi^{-1}\left(\frac{\dot{\bar{\varepsilon}}}{\gamma_0}\right)\right], \tag{2.11}$$

where

$$\sigma^* = \sigma_s - (\sigma_s - \sigma_0)\exp(-\delta\bar{\varepsilon}), \tag{2.12}$$

is the plastic strain-dependent yield stress due to the work-hardening effects [9]. In Eq. (2.12) σ_0 and σ_s denote the yield and saturation stress of the matrix material, γ_0 is the viscosity constant. We shall apply the linearized form of the relations (2.10) and (2.11), namely

$$\sigma_{\theta\theta} - \sigma_{rr} = -\Delta S = \sigma_s - (\sigma_s - \sigma_0)\exp(-\delta\bar{\varepsilon}) + \frac{\sigma_s}{\gamma_0}\dot{\bar{\varepsilon}}. \tag{2.13}$$

The integral of the above expressions has the form

$$\int_a^b \frac{-\Delta S}{r}dr = \sigma_s C_1 - (\sigma_s - \sigma_0)C_2 + \frac{\sigma_s}{\gamma_0}C_3, \tag{2.14}$$

where

$$C_1 = \int_a^b \frac{dr}{r} = \frac{1}{3}\ln\frac{1}{\xi}, \qquad C_3 = \int_a^b \frac{\dot{\bar{\varepsilon}}}{r}dr = \frac{2}{9}\frac{\dot{\xi}}{\xi}. \tag{2.15}$$

The integral

$$C_2 = \int_a^b \frac{\mathrm{e}^{-\delta\bar{\varepsilon}}}{r}dr = \int_a^b \mathrm{e}^{-\frac{2}{3}\delta\ln\frac{r^3}{r^3 - C(t)}}\frac{dr}{r} \tag{2.16}$$

has a non-elementary form, therefore we have to find its approximate value. We make the following change of variables in the expression (2.16):

$$x = 1 - \frac{C(t)}{r^3} \Rightarrow x_1 = 1 - \frac{C(t)}{a^3},\ x_2 = 1 - \frac{C(t)}{b^3} \text{ and } 0 < x_1 < x_2 < 1. \tag{2.17}$$

Thus the integral C_2 can be rewritten as follows:

$$C_2 = \frac{1}{3}\int_{x_1}^{x_2} \frac{x^{\frac{2}{3}\delta}}{1-x}dx. \tag{2.18}$$

The functions $f_1(x) = \dfrac{1}{1-x}$ and $f_2(x) = x^{\frac{2}{3}\delta}$ are continuous, bounded and integrable for all points from the interval $[x_1, x_2]$. Therefore, the mean value theorem for integrals gives

$$C_2 = \frac{1}{3}y^{\frac{2}{3}\delta}\int_{x_1}^{x_2}\frac{1}{1-x}dx = \frac{1}{3}\ln\frac{1}{\xi}y^{\frac{2}{3}\delta} = h(y) \quad \text{for } y \in [x_1, x_2]. \tag{2.19}$$

The function $h(y)$ is continuous and monotonic over the interval $[x_1, x_2]$ and it has the upper and lower bound values at the end points of this interval. Thus we have

$$\frac{1}{3}\ln\frac{1}{\xi}x_1^{\frac{2}{3}\delta} \leqslant h(y) \leqslant \frac{1}{3}\ln\frac{1}{\xi}x_2^{\frac{2}{3}\delta}. \tag{2.20}$$

The function $h(y)$ can be approximated by the mean value of the upper and lower bound values

$$h(y) \cong \frac{1}{6} \ln \frac{1}{\xi} \left(x_1^{\frac{2}{3}\delta} + x_2^{\frac{2}{3}\delta} \right) = \frac{1}{6} \ln \frac{1}{\xi} F(\xi, \xi_0), \tag{2.21}$$

where

$$F(\xi, \xi_0) = \left(\frac{\xi_0}{1-\xi_0} \frac{1-\xi}{\xi} \right)^{\frac{2}{3}\delta} + \left(\frac{1-\xi}{1-\xi_0} \right)^{\frac{2}{3}\delta}. \tag{2.22}$$

Finally, we obtain

$$C_2 = \frac{1}{6} \ln \frac{1}{\xi} F(\xi, \xi_0). \tag{2.23}$$

Substitution of the determined integrals and Eq. (2.2) into Eq. (2.10) gives the evolution equation for the porosity parameter in the following form:

$$\dot{\xi} = \frac{9}{4} \frac{\gamma_0}{\sigma_s} \frac{\xi}{1-\xi} \left\{ \bar{p} - p_g - \frac{1}{3}(1-\xi) \ln \frac{1}{\xi} [2\sigma_s - (\sigma_s - \sigma_0) F(\xi_0, \xi)] \right\}. \tag{2.24}$$

The equilibrium state is reached at $\dot{\xi} = 0$, thus

$$p_{\text{eq}} = p_g + \frac{1}{3}(1-\xi) \ln \frac{1}{\xi} [2\sigma_s - (\sigma_s - \sigma_0) F(\xi_0, \xi)]. \tag{2.25}$$

The relation of Eq. (2.25) shows a direct influence of the work-hardening effects on the value of the equilibrium pressure $p_{eq}(\xi)$ for particular porosity ξ.

For infinitesimal strains of the surrounding material, the strain-displacement relations may be written as follows [7]:

$$e_{rr} = \frac{\partial u}{\partial r}, \qquad e_{\varphi\varphi} = e_{\theta\theta} = \frac{u}{r}, \tag{2.26}$$

where

$$u = r - R = r - [r^3 - C(t)]^{1/3} \tag{2.27}$$

is the radial displacement. The infinitesimal equivalent strain and its rate are given by the expressions

$$\begin{aligned} \bar{\varepsilon} &= \frac{2}{3} \left(\frac{\partial u}{\partial r} - \frac{u}{r} \right) = \frac{2}{3} \left\{ \left[1 - \frac{C(t)}{r^3} \right]^{1/3} - \left[1 - \frac{C(t)}{r^3} \right]^{-2/3} \right\}, \\ \dot{\bar{\varepsilon}} &= -\frac{2}{3} \frac{\dot{C}(t)}{r^3} \left\{ \frac{1}{3} \left[1 - \frac{C(t)}{r^3} \right]^{1/3} + \frac{2}{3} \left[1 - \frac{C(t)}{r^3} \right]^{-2/3} \right\}. \end{aligned} \tag{2.28}$$

In this case, the derivation of an evolution equation for the porosity parameter is similar to the previous one. Thus, without going into details, we present the final result

$$\dot{\xi} = \frac{9}{4}\frac{\gamma_0}{\sigma_s \overline{F}_1(\xi_0,\xi)}\frac{\xi}{1-\xi} \left\{\overline{p} - p_g - \frac{1}{3}(1-\xi)\ln\frac{1}{\xi}[2\sigma_s - (\sigma_s - \sigma_0)\overline{F}(\xi_0,\xi)]\right\} \tag{2.29}$$

where

$$\overline{F}(\xi_0,\xi) = \exp\left\{\frac{2}{3}\delta\frac{\xi_0-\xi}{\xi(1-\xi_0)}\left[\frac{\xi_0(1-\xi)}{\xi(1-\xi_0)}\right]^{-2/3}\right\} + \exp\left[\frac{2}{3}\delta\frac{\xi_0-\xi}{1-\xi_0}\left(\frac{1-\xi}{1-\xi_0}\right)^{-2/3}\right],$$

$$\overline{F}_1(\xi_0,\xi) = \frac{1}{4}\frac{\xi}{\xi-\xi_0}\left(\frac{1-\xi}{1-\xi_0}\right)^{-2/3}\left\{\frac{1-\xi}{1-\xi_0}\left[1-\left(\frac{\xi_0}{\xi}\right)^{4/3}\right] + 8\left[1-\left(\frac{\xi_0}{\xi}\right)^{1/3}\right]\right\}. \tag{2.30}$$

It can be easily seen that the expressions (2.29) and (2.30) have a more complex structure than those obtained for finite deformation. Furthemore, the function $\overline{F}_1(\xi_0,\xi)$ has a singular point for the initial instant of the growth process ($\xi = \xi_0$). This property demands some additional activities in the numerical integration of the evolution equation (2.29). The proposed function (2.22) has no singular points. The comparison of the described solutions is shown in Figs. 3 and 4. Line *1* denotes the presented solution and line *2* denotes the geometrically linear solution [9]. The following material constants are assumed in numerical calculations:

$$\overline{p} = 800\text{MPa}, \quad p_g = 0, \quad \gamma_0 = 100\ \text{s}^{-1}, \quad \sigma_s = 350\ \text{MPa}, \quad \sigma_0 = 40\text{MPa}, \quad \delta = 5, \xi_0 = 0.001.$$

The curves in Fig. 3 illustrate the dependence of the equilibrium pressure p_{eq} on the porosity parameter ξ. The character of the analyzed quantity is the same for both discussed solutions. In the first phase of the void growth, the equilibrium pressure increases steadily to reach a maximal value, after that it decreases. Small quantitative differences occur at the maximum of p_{eq}. For a geometrically linearized solution the maximum of p_{eq} is greater than the corresponding value for the solution obtained.

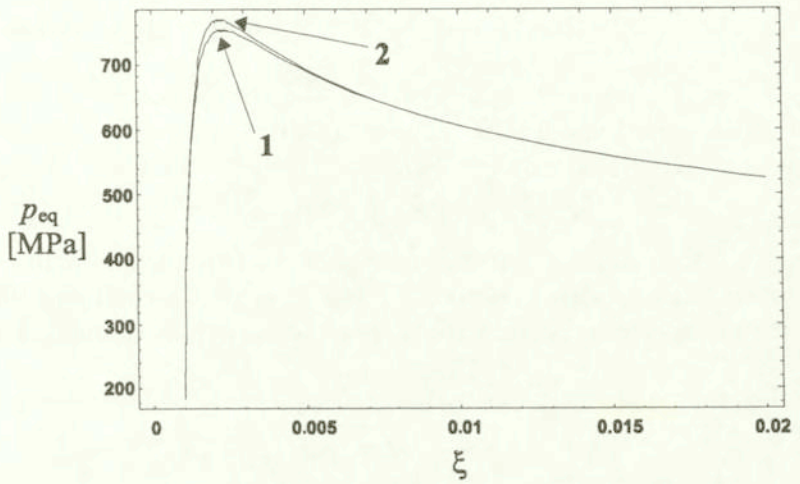

FIG. 3. Dependence of the equilibrium pressure p_{eq} on the porosity parameter ξ: line *1* – proposed solution, line *2* – geometrically linearized solution.

The evolution of the porosity is presented in Fig. 4. For this quantity the differences between the considered solutions are significant. For majority of metals, the loss of local carrying capacity is observed at $\xi \cong 0.3$. In the case of geometrically linear solution (line *2*) this value is reached in double time. This result is of great importance to the estimation of the fracture time for structural elements loaded monotonically.

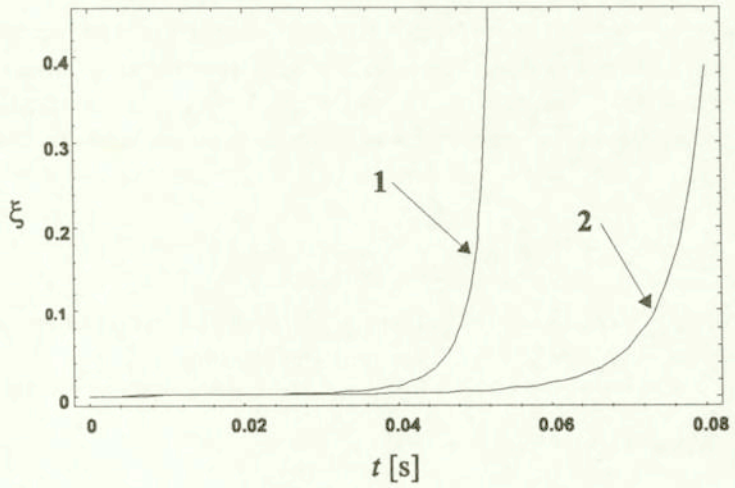

FIG. 4. Evolution of the porosity parameter ξ: line *1* – proposed solution, line *2* – geometrically linearized solution.

3. The microvoids growth equation for the complex state of stress

In the paper [11] the intensity invariant for the growth process in the complex state of stress was postulated in the following form:

$$I_g = b_1 J_1 + b_2 \sqrt{J_2'} + b_3 (J_3')^{1/3}, \tag{3.1}$$

where $b_i (i = 1, 2, 3)$ are the material constants, and by J_1 we denote the first invariant of the Cauchy stress tensor σ, J_2' and J_3' are the second and third invariants of the stress deviator, respectively. For the growth mechanism we assume [11]

$$\dot{\xi}_{\text{grow}} = \frac{g^*(\xi)}{T_m \sqrt{\sigma_0}} [I_g - \sigma_{\text{eq}}(\xi, \bar{\varepsilon}^p)], \tag{3.2}$$

where $T_m \sqrt{\sigma_0}$ denotes the dynamic viscosity of the material, $g^*(\xi)$ represents the void growth material function and allows for void interaction, and $\sigma_{\text{eq}}(\xi, \bar{\varepsilon}^p)$ is the porosity and equivalent plastic strain-depend void growth threshold stress.

Comparison of Eq. (2.24) and (3.2) shows that

$$\begin{aligned} g^*(\xi) &= c_1 \frac{\sqrt{\sigma_0}}{\sigma_s} \frac{\xi}{1 - \xi}, \\ \sigma_{\text{eq}}(\xi, \bar{\varepsilon}^p) &= c_2 (1 - \xi) \ln \frac{1}{\xi} [2\sigma_s - (\sigma_s - \sigma_0) F(\xi_0, \xi)]. \end{aligned} \tag{3.3}$$

The material constant c_1 controls the rate of growth and the material constant c_2 determines the level of the threshold stress. The constants σ_0 and σ_s denote the yield and saturation stress of the matrix material. The assumption that the growth process runs in domains of inelastic deformations leads to the particular relation

$$c_2 \geqslant \frac{1}{2(1 - \xi_0) \ln(1/\xi_0)}. \tag{3.4}$$

The evolution equation in the form (3.2) was also advantageous in certain problems of the plastic flow for cyclic dynamic loading [12].

4. Numerical example

The main objective of this example is the illustration of the fracture process in inelastic materials during dynamic loading. This kind of fracture can occur as a result of the shear-band localization generally attributed to a plastic instability

implied by microdamage softening during dynamic plastic flow process. In the dynamical initial-boundary value problem, the stress and deformation due to wave reflections and interactions are not uniformly distributed, and this kind of heterogeneity can lead to strain localization in the absence of geometrical or material irregularities [14].

The subject of the fracture numerical analysis is a thin rectangular steel plate, Fig. 5a.

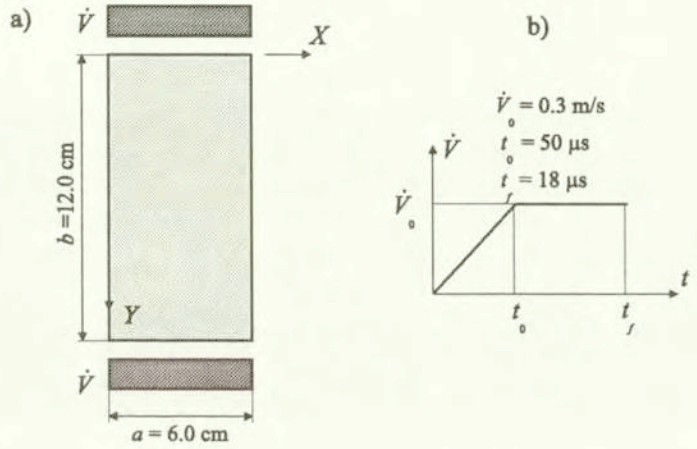

FIG. 5. Dimensions of the plate and variation in time of the kinematic constraints.

The shorter edges of the plate have been subjected to the tensile kinematic constraints, Fig. 5b. The rate-dependent material was assumed, and the effect of the plastic work-hardening was omitted. The porosity evolution has been described by Eq. (3.2) in which the proposed function $F(\xi, \xi_0)$ (2.22) was used. The initial-boundary value problem of this type was the subject of an experimental investigation [13], as well as of a numerical analysis by the finite element method [14]. In the paper [13], different fracture types of sheet specimens were investigated. The plane stress and plane strain conditions were assumed. It was confirmed that the variations in specimen geometry produce significant changes in the stress state, directions of shear bands and in ductility. The final fracture of the plate occurred in the shear bands. Numerical solutions presented in the paper [14] have been obtained by the finite element method. Particular attention has been focused on the thin shear band region of finite width, which undergoes significant deformations and temperature rise. The numerical results are compared with the available experimental observation data.

In this paper we have restricted our attention to the presentation of our own numerical results. Interesting aspects of the initial-boundary problem formulation and of the applied finite difference method have been omitted.

Figure 6 illustrates the evolution of an equivalent plastic deformation in the discretized domain of the plate. In the initial phase of deformation the shear effects (white bands) occur in the region adjacent to the loaded edges. With continued loading process, two cross shear-bands are developed in the center of the plate. Numerical experiments have revealed that the final distribution of shear bands also depends on the rate of deformation, not only on the plate geometry. For the rates larger than those assumed in the example, the shear bands develop in the region adjacent to the loaded edges.

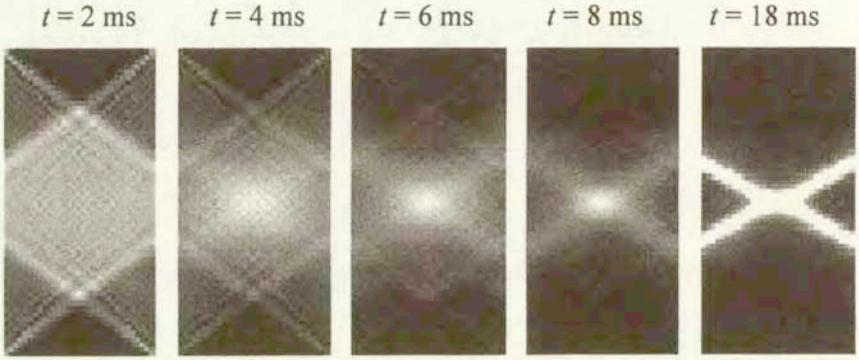

FIG. 6. Evolution of the equivalent plastic deformation in the discretized domain of the plate.

In Fig. 7 we present the distribution of the equivalent plastic deformation along the cross-section $X = a/4$ for chosen instants of the deformation process. It can be observed that the plastic strains develop in the zones of localized viscoplastic flow. The width of these zones does not tend to singular lines as for rate-independent models and depends significantly on the viscosity, which is used in calculations [14]. The obtained results are in good agreement with the experimental observations of CHAKRABARTI and SPERTNAK [13].

The porosity evolution corresponding to the evolution of equivalent plastic deformation (Fig. 7) is shown in Fig. 8.

It can be seen that the intensive increase in the porosity in shear bands occurs shortly before the final fracture of the plate. The process of the void growth, as well as of its coalescence, leads to the nucleation of a macrocrack. The development of macrocracks is illustrated in Fig. 9 by means of three selected instants of the deformation process. The cracking started in the center of a plate, and with continued loading process the macrocraks develop along the shear bands. The deformed configuration for final fracture of a plate ($t_f = 18$ ms) is shown in Fig. 10. Figure 11 shows the variation in time of the porosity parameter ξ_{grow} at the mid-point of a plate. This variation is interesting from the viewpoint of

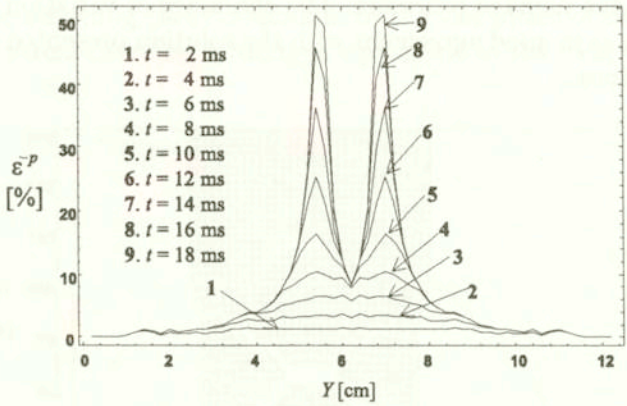

FIG. 7. Distribution of the equivalent plastic deformation along the cross-section $X = a/4$ for chosen instants of the deformation process.

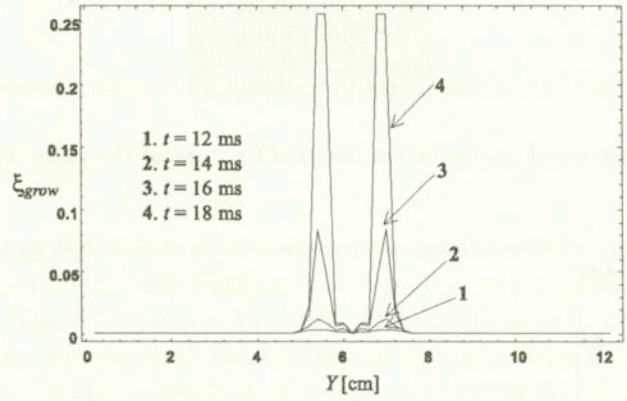

FIG. 8. Distribution of porosity along the cross-section $X = a/4$ for chosen instants of the deformation process.

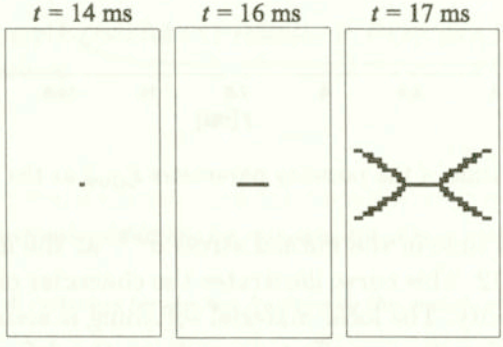

FIG. 9. Development of a macrocrack (black domains).

the analysis of the damage processes. The character of variation of the porosity parameter ξ_{grow} is in good agreement with the solution presented in Section 2 for finite deformations.

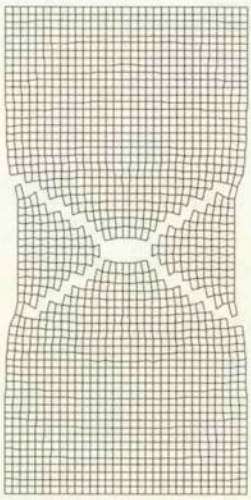

FIG. 10. Deformed configuration for final fracture of the plate, $t_f = 18$ ms.

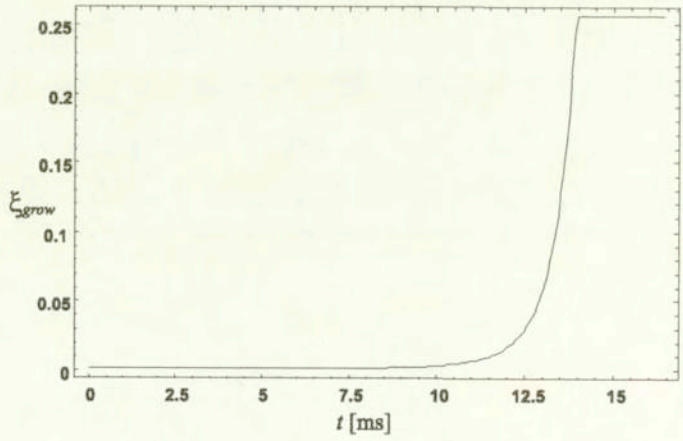

FIG. 11. Variation in time of the porosity parameter ξ_{grow} at the midpoint of the plate.

The variation in time of the normal stress σ^{YY} at the midpoint of the plate is presented in Fig. 12. This curve illustrates the character of changes of the local stress-carrying capacity. The local material softening is seen in the behaviour of inelastic strains. This softening effect depends on the deformation (geometrical softening), as well as on the porosity evolution (physical softening). It can be seen

that the physical softening effect dominates in the last phase of deformations. A complete loss of stress-carrying capacity is equivalent to the local fracture of the material.

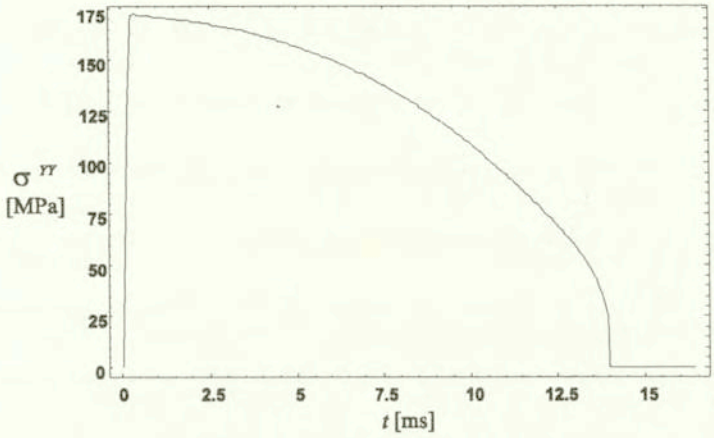

FIG. 12. Variation in time of the normal stress σ^{YY} at the midpoint of the plate.

5. Conclusions

On the basis of the hollow sphere model, the void growth equation has been derived for inelastic finite deformation. This equation has a simple form without singular points. These properties have practical significance in numerical applications. From the viewpoint of the analysis of fracture processes, the proposed evolution equation makes possible a more accurate estimation of fracture course and time for structural elements.

Acknowledgements

The author is sincerely grateful to Professor P. PERZYNA for many interesting and invaluable discussions.

References

1. P. PERZYNA, *The constitutive equations for rate-sensitive plastic materials*, Q. Appl. Math., **20**, 321, 1963.
2. F.A. MCCLINTOCK, *A criterion for ductile fracture by the growth of holes*, J. Appl. Mech., **35**, 363, 1968.
3. J.R. RICE, D.M. TRACEY, *On the ductile enlargement of voids in triaxial stress fields*, J. Mech. Phys. Solids, **17**, 201, 1969.

4. B. BUDIANSKY, J.W. HUTCHINSON, S. SLUTSKY, *Void growth and collapse in viscous solids*, H.G. Hokins, M.J. Sewell, Eds., Mechanics of solids, Pergamon Press, Oxford 1982, 13.

5. Y. HUANG, J.W. HUTCHINSON, V. TVERGAARD, *Cavitation instabilities in elastic-plastic solids*, J. Mech. Phys. Solids, **39**, 223, 1991.

6. M.M. CARROLL, A.C. HOLT, *Static and dynamic pore-collapse relations for ductile porous materials*, J. Appl. Phys., **43**, 1626, 1972.

7. J.N. JOHNSON, *Dynamic fracture and spallation in ductile solids*, J. Appl. Phys., **52**, 2812, 1981.

8. P. PERZYNA, *Internal state variable description of dynamic fracture of ductile solids*, Int. J. Solids Structures, **22**, 797, 1986.

9. J.A. NEMES, J. EFTIS, *Constitutive modeling of the dynamic fracture of smooth tensile bars*, Int. J. Plasticity, **9**, 243, 1993.

10. P. PERZYNA, A. DRABIK, *Influence of thermal effects on micro-damage mechanism in dynamic processes*, Arch. Mech., **40**, 795, 1988.

11. P. PERZYNA, *Constitutive modelling for brittle dynamic fracture in dissipative solids*, Arch. Mech., **38**, 725, 1986.

12. W. DORNOWSKI, P. PERZYNA, *Constitutive modelling of inelastic solids for plastic flow process under cyclic dynamic loading*, 32nd Solid Mechanics Conference, Zakopane, September 1-5, 1998.

13. A.K. CHAKRABARTI, J.W. SPRETNAK, *Instability of plastic flow in the directions of pure shear. II Experimental*, Metallurgical Transactions, **6A** (1975), 1975.

14. T. ŁODYGOWSKI, P. PERZYNA, *Localized fracture in inelastic polycrystalline solids under dynamic loading processes*, Int. J. Damage Mechanics, **6**, 364, 1997.

Received September 16, 1998; new version November 25, 1998.